

# Transverse spatial and frequency properties of two-photon states generated by spontaneous parametric down-conversion

A. G. da Costa Moura, W. A. T. Nogueira, and C. H. Monken  
*Departamento de Física, Universidade Federal de Minas Gerais,  
Caixa Postal 702, Belo Horizonte, MG 30123-970, Brazil*

S. P. Walborn  
*Instituto de Física, Universidade Federal do Rio de Janeiro,  
Caixa Postal 68528, Rio de Janeiro, RJ 21945-970, Brazil*

(Dated: November 6, 2018)

We present a detailed account of the two-photon states generated by SPDC in both type I and type II phase matching, including the effects of anisotropy of the nonlinear medium and the frequency spread of the down-converted fields. Accurate as well as simplified expressions are derived for type I and type II phase matching in the context of Fourier Optics. The main results are compared with experimental data available in the literature, showing good agreement in all cases.

PACS numbers: 42.65.Lm, 42.50.Dv, 42.65.Ex

## I. INTRODUCTION

In the course of the last three decades, spontaneous parametric down-conversion (SPDC) has proven to be a valuable tool in the experimental investigation of fundamental properties of the electromagnetic field in the quantum domain [1, 2, 3], including nonclassical correlations, entanglement and nonlocality. The fact that SPDC is capable of generating pairs of photons in a wide range of frequencies and wave vectors, in addition to the fact that these photons may be entangled in a number of different degrees of freedom, qualifies SPDC also as a unique tool in the demonstration of quantum information procedures and protocols [4].

In many applications, especially in the pioneering ones, a basic knowledge of a few properties of the two-photon states generated by SPDC is enough to explain the effects discussed. As the applications become more sophisticated, for example in those that combine correlations in more than one degree of freedom, a more comprehensive approach is necessary in order to enhance the capabilities of quantum state engineering. In this direction, the use of Fourier Optics concepts in two-photon optics represents a significant step.

An important application field of SPDC is the construction of entangled photon state sources with high fidelity and purity [5, 6, 7, 8, 9, 10, 11, 12]. In order to obtain efficient and dependable two-photon sources, a number of questions must be addressed, as for example, phase compensation, mode coupling, pair collection efficiency, maximum photon flux, etc. To be optimized, all these points require a detailed knowledge of the SPDC process.

Another context in which a more precise model is crucial refers to the issue of conservation of orbital angular momentum (OAM) of light in the process of SPDC [13, 14, 15, 16, 17, 18, 19]. Oversimplifications or inconsistent assumptions about the two-photon state gener-

ated have led to conflicting conclusions on whether OAM is conserved or not in SPDC.

In this work, we present a detailed account of the two-photon states generated by SPDC in both type I and type II phase matching, including the effects of anisotropy of the nonlinear medium and the frequency spread of the down-converted fields. As an exact approach to this problem presents a considerable level of difficulty, we are forced to restrict ourselves to some approximations. We adhere to the commonly adopted simplified procedure for the quantization of the electromagnetic field in the nonlinear medium by just multiplying the  $\mathbf{k}$  vectors by the corresponding refractive indices and keeping the vacuum expressions for the field operators. The frequency spread of the down-converted fields is considered to be small compared to their central frequencies. We also work in the paraxial approximation, in which the propagation of the fields is much easier to deal with. Fortunately, these approximations, are good enough to encompass a great number of practical cases. We admit, however, that while the model discussed here is helpful in far field applications, it may not be appropriate in discussions of the fundamental interactions inside the nonlinear medium. Whenever possible, the results reported here are compared with experimental data, obtained in our labs or reported in the literature.

It should be mentioned that other authors have reported their contributions to this field, in different levels of detail and scope [13, 18, 20, 21, 22, 23, 24, 25, 26, 27, 28]. From our point of view, a comprehensive description of SPDC that accounts for all features observed so far in two-photon states, with expressions ready to use in Fourier optics, is still missing. It is in this context that we present our work.

## II. TWO-PHOTON STATE GENERATED BY SPDC

The interaction Hamiltonian describing the optical processes of parametric down-conversion in nonlinear birefringent crystals is usually written in terms of a simplified field quantization in matter [29]. The field modes participating in this process are coupled by the second-order susceptibility tensor  $\chi^{(2)}$ . Due to the phase matching conditions, the coupling occurs only for some sets of polarizations, known as type I and type II. In negative uniaxial crystals ( $n_e < n_o$ ) such as BBO ( $\beta$ -BaB<sub>2</sub>O<sub>4</sub>) and Lithium Iodate (LiIO<sub>3</sub>), the down-conversion process with type I phase matching can be summarized as  $e \rightarrow oo$ , meaning that one photon of the pump beam with extraordinary polarization is converted into two photons with ordinary polarization. In type II phase matching, the process is represented by  $e \rightarrow oe$  or  $e \rightarrow eo$ .

In a perturbative approach, the (post-selected) two-photon state generated by SPDC is written as [20]

$$|\Psi\rangle = \sum_{\sigma_1, \sigma_2} \sum_{\mathbf{k}_1, \mathbf{k}_2} \Phi_{\mathbf{k}_p \mathbf{k}_1 \mathbf{k}_2 \sigma_p \sigma_1 \sigma_2} |\mathbf{k}_1, \sigma_1\rangle |\mathbf{k}_2, \sigma_2\rangle, \quad (1)$$

where  $\mathbf{k}_1$  and  $\mathbf{k}_2$  are the wave vectors of the down-converted fields,  $\mathbf{k}_p$  is the wave vector of the pump field, whose frequency  $\omega_p$  is assumed to be well defined.  $\sigma_j$  indicates the polarization of each down-converted field, that can be ordinary ( $o$ ) or extraordinary ( $e$ ), and  $|\mathbf{k}_j, \sigma_j\rangle$  represent a one-photon state in the plane wave mode  $\mathbf{k}_j, \sigma_j$ . Considering that the nonlinear crystal is a rectangular block of sides  $L_x, L_y, L_z$ , with two faces parallel to the plane  $xy$ , the amplitude  $\Phi$  is given by

$$\begin{aligned} \Phi_{\{\mathbf{k}, \sigma\}} &= g_{\mathbf{k}_p, \sigma_p} g_{\mathbf{k}_1, \sigma_1}^* g_{\mathbf{k}_2, \sigma_2}^* \tau e^{i\Omega(t - \frac{\tau}{2})} \text{sinc} \frac{\Omega \tau}{2} \\ &\times \sum_{i, j, k=x, y, z} \tilde{\chi}_{ijk}^{(2)}(\hat{\mathbf{e}}_{\mathbf{k}_0, \sigma_0})_i (\hat{\mathbf{e}}_{\mathbf{k}_1, \sigma_1})_j^* (\hat{\mathbf{e}}_{\mathbf{k}_2, \sigma_2})_k^* \\ &\times \mathcal{E}_{\mathbf{k}_p, \sigma_p} \int_{\mathcal{I}} e^{-i\Delta \cdot \mathbf{r}} d\mathbf{r}, \end{aligned} \quad (2)$$

where  $\{\mathbf{k}, \sigma\}$  represents the set of indices  $\mathbf{k}_p \mathbf{k}_1 \mathbf{k}_2 \sigma_p \sigma_1 \sigma_2$ ,  $g_{\mathbf{k}_j, \sigma_j} = i \left[ \frac{\hbar \omega_j}{2\epsilon_0 V n^2(\mathbf{k}_j, \sigma_j)} \right]^{\frac{1}{2}}$ ,  $V$  is the quantization volume,  $\mathcal{I}$  is the interaction volume ( $L_x L_y L_z$ ),  $n(\mathbf{k}_j, \sigma_j)$  is the refractive index corresponding to the mode  $\mathbf{k}_j, \sigma_j$ ,  $\Omega = \omega_1 + \omega_2 - \omega_p$ ,  $\tau$  is the interaction time,  $\tilde{\chi}_{ijk}^{(2)}$  is related to the second-order nonlinear susceptibility tensor [29],  $(\hat{\mathbf{e}}_{\mathbf{k}_i, \sigma_i})_j$  ( $j = x, y, z$ ) are the cartesian components of the polarization vectors,  $\mathcal{E}_{\mathbf{k}_p, \sigma_p}$  is the pump field amplitude in the mode  $\mathbf{k}_p, \sigma_p$ , and  $\Delta = \mathbf{k}_1 + \mathbf{k}_2 - \mathbf{k}_p$ .

In order to simplify expression (2), it is convenient to make the following approximations:

(a) The pump frequency  $\omega_p$  is well defined and the interaction time is long, so that the term  $\text{sinc} \Omega \tau / 2$  is significant only when  $\omega_1 + \omega_2 = \omega_p$ . The frequencies  $\omega_1$

and  $\omega_2$  can therefore be written as

$$\omega_1 = \frac{\omega_p}{2} (1 + \nu), \quad (3a)$$

$$\omega_2 = \frac{\omega_p}{2} (1 - \nu). \quad (3b)$$

This assumption can be justified by the use of a moderate power continuous-wave pump laser so that the time interval between two down-conversions is large compared to the detection resolving time.

(b) The frequency spread of the detectable down-converted fields is small compared to the central frequency ( $|\nu| \ll 1$ ), so that the dispersion of the refractive indices around the central frequency  $\omega_p/2$  is small and a linear approximation can be used. This assumption is justified by the use of narrow-band interference filters in front of the detectors. For example, for a 100nm wavelength spread centered at 700nm,  $\nu$  lies in the interval  $(-0.08, 0.08)$ .

(c) The terms  $g_{\mathbf{k}_j, \sigma_j}$  and  $\tilde{\chi}_{ijk}^{(2)}$  are slowly-varying functions of  $\mathbf{k}_j$ , so that they may be taken as constants in the intervals considered for  $\mathbf{k}_j$ .

(d) The pump beam propagates along the  $z$  axis and the crystal is large enough in the  $x$  and  $y$  directions to contain the whole pump beam transverse profile. In this case,  $L_x$  and  $L_y$  can be extended to infinity and the last term in expression (2), the integral  $\int_{\mathcal{I}} e^{-i\Delta \cdot \mathbf{r}} d\mathbf{r}$ , is proportional to

$$\delta(k_{1x} + k_{2x} - k_{px}) \delta(k_{1y} + k_{2y} - k_{py}) \int_{z_c - L_z/2}^{z_c + L_z/2} e^{-i\Delta_z z} dz,$$

where  $z_c$  locates the center of the crystal.

(e) The quantization volume is large enough to justify the replacement of summations in  $\mathbf{k}$  by integrals.

(f) The pump beam contains only extraordinary polarization. It is implicit in this assumption that we are dealing with negative birefringent crystals.

Under the above assumptions, Eq. (1) is written as

$$\begin{aligned} |\Psi\rangle &= \sum_{\sigma_1, \sigma_2} \int d\nu \int d\mathbf{q}_1 \int d\mathbf{q}_2 \Phi_{\sigma_1 \sigma_2}(\mathbf{q}_1, \mathbf{q}_2, \nu) \\ &\times |\mathbf{q}_1, \nu, \sigma_1\rangle |\mathbf{q}_2, -\nu, \sigma_2\rangle, \end{aligned} \quad (4)$$

where  $|\mathbf{q}_j, \nu, \sigma_j\rangle$  represents a one-photon state in the mode defined by the transverse ( $xy$ ) component  $\mathbf{q}_j$  of the wave vector, the frequency  $(1 + \nu)\omega_p/2$  and by the polarization  $\sigma_j$ . The amplitude  $\Phi$  is now reduced to

$$\Phi_{\sigma_1 \sigma_2} \approx C_{\sigma_1 \sigma_2} G(\nu) \tilde{\mathcal{E}}(\mathbf{q}_1 + \mathbf{q}_2) \int_{z_c - L_z/2}^{z_c + L_z/2} e^{-i\Delta_z z} dz, \quad (5)$$

where  $C_{\sigma_1 \sigma_2}$  is a coupling constant, which depends on the nonlinear susceptibility tensor,  $G(\nu)$  is the spectral function defined by the narrow bandwidth filters placed in front of the detectors, and  $\tilde{\mathcal{E}}$  is the plane wave spectrum of the pump beam  $\tilde{\mathcal{E}}(\mathbf{q}_p)$ , with  $\mathbf{q}_p$  replaced by  $\mathbf{q}_1 + \mathbf{q}_2$ .

The integral in  $z$  is discussed in what follows. The function  $G(\nu)$  may be centered at zero in frequency degenerate configurations or at some fixed small detuning  $\nu_0$ .

Most of the properties of the down-converted fields is determined by the longitudinal wave vector mismatch

$$\Delta_z = k_{1z} + k_{2z} - k_{pz}. \quad (6)$$

If the anisotropy of the medium is neglected (which is not always convenient),  $\nu = 0$  (monochromatic approximation), and the crystal is cut for collinear phase matching,  $\Delta_z$  has a simple expression in terms of  $\mathbf{q}_1$  and  $\mathbf{q}_2$ , with the  $z$  components replaced by  $k_{jz} = \sqrt{|\mathbf{k}_j|^2 - |\mathbf{q}_j|^2}$ . In the paraxial approximation,  $k_{jz}$  can be approximated by  $k_{jz} \approx |\mathbf{k}_j| - |\mathbf{q}_j|^2/2|\mathbf{k}_j|$ . This leads, for  $z_c = 0$ , to

$$\int_{-L_z/2}^{+L_z/2} e^{-i\Delta_z z} dz \propto \text{sinc} \left( \frac{L_z}{4|\mathbf{k}_p|} |\mathbf{q}_1 - \mathbf{q}_2|^2 \right),$$

which appears in the amplitude reported in Ref. [30]. This result, however, is a good approximation only when the crystal is very thin, the diffraction (Rayleigh) length  $z_o$  of the pump beam is large, and the detection area is small so that the sinc function can be approximated by 1. In more general conditions, the anisotropy of the crystal must be taken into account.

From this point on, we will refer to the arrangement depicted in Fig.1.

### III. THE EFFECT OF ANISOTROPY

Let us consider a monochromatic electromagnetic field in a plane wave mode  $e^{i(\mathbf{k}\cdot\mathbf{r}-\omega t)}$  propagating through a nonmagnetic uniaxially birefringent medium with ordinary and extraordinary refractive indices  $n_o$  and  $n_e$ , respectively. Considering that the optic axis lies on the plane  $xz$ , making an angle  $\theta$  with the  $z$  direction, and that the plane wave has extraordinary polarization, Maxwell's equations require that the components of the wave vector  $\mathbf{k}$ , whose cartesian components are  $(q_x, q_y, k_z)$ , satisfies the *ray surface* equation [31]

$$(n_o^2 \cos^2 \theta + n_e^2 \sin^2 \theta) q_x^2 + (n_o^2 \sin^2 \theta + n_e^2 \cos^2 \theta) k_z^2 + 2(n_o^2 - n_e^2) \sin \theta \cos \theta q_x k_z + n_o^2 q_y^2 = \left( n_o n_e \frac{\omega}{c} \right)^2. \quad (7)$$

Solving Eq. (7) for  $k_z$ , we find

$$k_z = -\alpha q_x + \sqrt{\varkappa^2 - \beta q_x^2 - \gamma q_y^2}, \quad (8)$$

where

$$\alpha = \frac{(n_o^2 - n_e^2) \sin \theta \cos \theta}{n_o^2 \sin^2 \theta + n_e^2 \cos^2 \theta}, \quad (9)$$

$$\beta = \left( \frac{n_o n_e}{n_o^2 \sin^2 \theta + n_e^2 \cos^2 \theta} \right)^2, \quad (10)$$

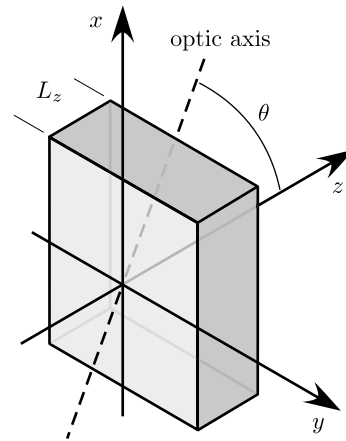


FIG. 1: Geometry of the problem. The uniaxial medium is assumed to be a slab of thickness  $L_z$ , having its faces parallel to the  $xy$  plane. The optic axis lies in the  $xz$  plane, at an angle  $\theta$  with the  $z$  direction.

$$\gamma = \frac{n_o^2}{n_o^2 \sin^2 \theta + n_e^2 \cos^2 \theta}, \quad (11)$$

$$\varkappa = \eta \frac{\omega}{c}, \quad (12)$$

with

$$\eta = \frac{n_o n_e}{\sqrt{n_o^2 \sin^2 \theta + n_e^2 \cos^2 \theta}}. \quad (13)$$

The ordinary and extraordinary refractive indices  $n_o$  and  $n_e$  are obtained from the Sellmeier equations. For BBO,  $n_o$  and  $n_e$  are obtained from [32]

$$n_o^2 = 2.7359 + \frac{0.01878}{\lambda^2 - 0.01822} - 0.01354 \lambda^2, \quad (14a)$$

$$n_e^2 = 2.3753 + \frac{0.01224}{\lambda^2 - 0.01667} - 0.01516 \lambda^2, \quad (14b)$$

with  $\lambda$  given in  $\mu\text{m}$ . For Lithium Iodate we use [33]

$$n_o^2 = 2.083648 + \frac{1.332068 \lambda^2}{\lambda^2 - 0.035306} - 0.008525 \lambda^2, \quad (15a)$$

$$n_e^2 = 1.673463 + \frac{1.245229 \lambda^2}{\lambda^2 - 0.028224} - 0.003641 \lambda^2. \quad (15b)$$

Within the paraxial approximation,

$$k_z \approx \varkappa - \alpha q_x - \frac{1}{2\varkappa} (\beta q_x^2 + \gamma q_y^2). \quad (16)$$

The term  $\alpha$  represents a linear displacement in the  $x$  direction, also known as the *walk-off*. It reaches its maximum value in the neighborhood of  $\theta = 45^\circ$ . The terms  $\beta$  and  $\gamma$  account for the deviation of the curvatures of the ray surface from a spherical surface in the  $x$  and  $y$  directions, respectively. Differently from  $\alpha$ , the terms  $\beta$  and  $\gamma$

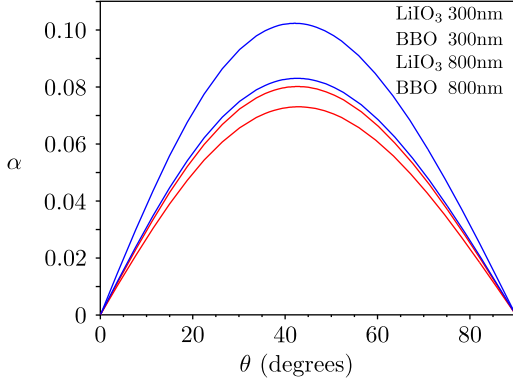


FIG. 2: (Color online) Values of  $\alpha$  for for 300nm and 600nm in BBO and Lithium Iodate as functions of the phase matching angle  $\theta$ . The curves are ordered from top to bottom, according to the legend.

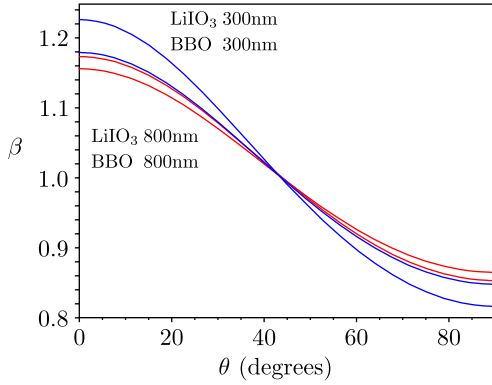


FIG. 3: (Color online) Values of  $\beta$  for for 300nm and 600nm in BBO and Lithium Iodate as functions of the phase matching angle  $\theta$ . The curves are ordered from top to bottom, according to the legend.

have little influence in the phase matching. The term  $\eta$  is the refractive index for a plane wave with extraordinary polarization, propagating along the  $z$  direction, whose wavenumber is  $\varkappa$ . Figs. 2, 3 and 4 show the values of  $\alpha$ ,  $\beta$  and  $\gamma$  as functions of the phase matching angle  $\theta$  for 300nm and 600nm in BBO and Lithium Iodate.

#### IV. TYPE I PHASE MATCHING

Let us consider first the case of type I phase matching, where the pump field has extraordinary polarization and the down-converted fields have ordinary polarization ( $e \rightarrow oo$ ). In this case,

$$k_{pz} \approx \varkappa_p - \alpha_p q_{px} - \frac{1}{2\varkappa_p} (\beta_p q_{px}^2 + \gamma_p q_{py}^2), \quad (17)$$

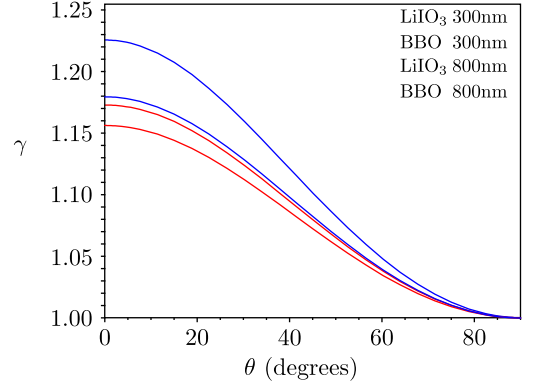


FIG. 4: (Color online) Values of  $\gamma$  for for 300nm and 600nm in BBO and Lithium Iodate as functions of the phase matching angle  $\theta$ . The curves are ordered from top to bottom, according to the legend.

$$k_{1z} \approx k_1 - \frac{q_1^2}{2k_1}, \quad (18)$$

$$k_{2z} \approx k_2 - \frac{q_2^2}{2k_2}, \quad (19)$$

where  $k_1 = n_{o1} \omega_1 / c$  and  $k_2 = n_{o2} \omega_2 / c$ . Since we are assuming  $\nu \ll 1$ , the refractive indices  $n_{o1}$  and  $n_{o2}$  can be written in a linear approximation as

$$n_{o1} = \bar{n}_o (1 + a\nu), \quad (20a)$$

$$n_{o2} = \bar{n}_o (1 - a\nu), \quad (20b)$$

where  $\bar{n}_o$  is the ordinary refractive index at the frequency  $\omega_p/2$ , and factor  $a$  is given by

$$a = \frac{\omega_p}{2\bar{n}_o} \left. \frac{dn_o}{d\omega} \right|_{\omega=\omega_p/2}. \quad (21)$$

In order to calculate  $\Delta_z$ , which in type I phase matching will be referred to as  $\Delta_z^{oo}$ , we have to write  $k_{1z} + k_{2z} - k_{pz}$  replacing  $q_{px}$  and  $q_{py}$  in Eq. (17) by  $q_{1x} + q_{2x}$  and  $q_{1y} + q_{2y}$ , respectively. After some manipulation, we find

$$\begin{aligned} \Delta_z^{oo} \approx & K\mu_{oo} + \alpha_p(q_{1x} + q_{2x}) \\ & - \frac{1}{\bar{n}_o K} \left[ \frac{q_1^2}{1+\nu} + \frac{q_2^2}{1-\nu} \right. \\ & \left. - \frac{b}{2}(q_{1x} + q_{2x})^2 - \frac{g}{2}(q_{1y} + q_{2y})^2 \right], \end{aligned} \quad (22)$$

where  $K = \omega_p / c$ ,  $b = \beta_p \bar{n}_o / \eta_p$ , and  $g = \gamma_p \bar{n}_o / \eta_p$ . The subscript  $p$  means that  $\alpha$ ,  $\beta$  and  $\gamma$  refer to the pump field.  $\mu_{oo}$  is the type I *collinear index mismatch*, defined as

$$\mu_{oo} = \bar{n}_o (1 + a\nu^2) - \eta_p. \quad (23)$$

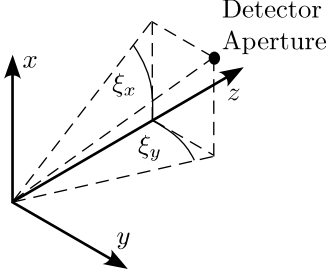


FIG. 5: Angular components of the down-converted fields.

In the derivation of Eq. (22), terms in  $\nu^2$  were neglected with respect to  $\nu$ . For type I collinear ( $\mu_{oo} = 0$ ) phase matching in BBO pumped with  $\lambda_p = 351\text{nm}$ ,  $\alpha_p = 0.0747$ ,  $a = 0.02$ ,  $b = 1.06$ , and  $g = 1.11$ . For Lithium Iodate,  $\alpha_p = 0.0871$ ,  $a = 0.03$ ,  $b = 0.951$  and  $g = 1.07$ .

Sometimes, instead of the transverse components of the wave vectors, one is interested in the output angles of the down-converted photons. In general, the output fields of interest propagate at small angles with respect to the  $z$  axis, so that one can approximate the output angles by

$$\xi_{1j} \approx \frac{c}{\omega_1} q_{1j} = \frac{2q_{1j}}{(1+\nu)K}, \quad (24a)$$

$$\xi_{2j} \approx \frac{c}{\omega_2} q_{2j} = \frac{2q_{2j}}{(1-\nu)K}, \quad (24b)$$

where  $j = x, y$ , and we define the vectors  $\xi_1 = (\xi_{1x}, \xi_{1y})$  and  $\xi_2 = (\xi_{2x}, \xi_{2y})$  as shown in Fig. 5. In the far field,  $\xi_1$  and  $\xi_2$  can be written in terms of the transverse coordinates  $\rho_1$  and  $\rho_2$  of the detectors as

$$\xi_1 \approx \frac{1}{z_D} \rho_1, \quad (25a)$$

$$\xi_2 \approx \frac{1}{z_D} \rho_2, \quad (25b)$$

where  $z_D$  is the  $z$  coordinate of the detection plane (parallel to the  $xy$  plane).

In terms of the angular variables  $\xi_1$  and  $\xi_2$ , the amplitude  $\Phi_{oo}$ , defined in Eq. (5), is written as

$$\begin{aligned} \Phi_{oo} \approx & N G(\nu) \tilde{\mathcal{E}} \left[ \frac{K}{2} (\xi_1 + \xi_2) + \frac{K\nu}{2} (\xi_1 - \xi_2) \right] \\ & \times \text{sinc} \left[ \frac{KLz}{2} f_{oo}(\xi_1, \xi_2, \nu) \right] \\ & \times \exp[-iKz_c f_{oo}(\xi_1, \xi_2, \nu)], \end{aligned} \quad (26)$$

where  $N$  is a normalization constant and

$$\begin{aligned} f_{oo}(\xi_1, \xi_2, \nu) = & \mu_{oo} + \frac{\alpha_p}{2} [(1+\nu)\xi_{1x} + (1-\nu)\xi_{2x}] \\ & - \frac{1}{4\bar{n}_o} \left\{ (1+\nu)\xi_1^2 + (1-\nu)\xi_2^2 \right. \\ & - \frac{b}{2} [(1+\nu)\xi_{1x} + (1-\nu)\xi_{2x}]^2 \\ & \left. - \frac{g}{2} [(1+\nu)\xi_{1y} + (1-\nu)\xi_{2y}]^2 \right\}. \end{aligned} \quad (27)$$

The single count rate as a function of  $\xi_1$  ( $\xi_2$ ) and  $\nu$  can be obtained from Eq. (26) by integration in  $\xi_2$  ( $\xi_1$ ). To show that Eqs. (26) and (27) describe the correct dependence of  $\Phi$  on frequency and output angles, the output angle  $\xi_x$  is plotted as a function of the down-converted wavelength in Fig. 6 for a 15mm-long Lithium Iodate crystal pumped by a 325nm laser beam for three different values of the phase matching angle  $\theta$ . Results for  $\theta = 59.217^\circ$  (collinear) and  $\theta = 59.185^\circ$  are in good agreement with experimental data reported by Bogdanov *et al.* [34] for  $\theta = 59.22^\circ$  and  $\theta = 58.97^\circ$ , respectively. The difference of  $0.22^\circ$  in the noncollinear phase matching angle is probably due to the fact that the noncollinear condition is obtained by tilting the crystal.

The two-photon frequency spectral content of  $\Phi_{oo}$  for a given pair of selected output angles  $\xi_1^o$  and  $\xi_2^o$  can also be derived from Eq. (26). Experimentally, this spectrum can be directly measured [25], or inferred from the Hong-Ou-Mandel dip when the measurement is taken with broadband filters. The expected profile of the coincidence detection probability as a function of the path length difference  $\delta l = c\delta\tau$  in a Hong-Ou-Mandel interferometer is given by [35]

$$P_c(\delta\tau) = \frac{1}{2} \left[ 1 - \frac{\int d\tau \tilde{\phi}^*(\tau) \tilde{\phi}(\tau - \delta\tau)}{\int d\tau |\tilde{\phi}|^2(\tau)} \right], \quad (28)$$

where, for a pump beam with a symmetric transverse profile,

$$\tilde{\phi}(\tau) = \int d\nu \Phi_{oo}(\xi_1^o, \xi_2^o, \nu) e^{-iK\nu c\delta\tau}. \quad (29)$$

The integrals are taken from  $-\infty$  to  $\infty$ . Fig. 7 shows a plot of  $P_c(\delta\tau)$  calculated with Eqs. (26) and (28), for a BBO crystal with  $L_z = 1\text{mm}$  in type I phase matching, pumped by a 351nm laser, without interference filters. The collection angles are such that both down-converted beams are centered at 702nm.

In the collinear detection configuration ( $\xi_1 = \xi_2 = 0$ ), the spectral profile of the two-photon state depends on the phase matching angle  $\theta$ . Figures 8 and 9 show the down-converted wavelengths for collinear type I phase matching as a function of  $\delta\theta$ , the deviation from  $\theta_m = 51.704^\circ$  for Lithium Iodate and from  $\theta_m = 33.543^\circ$  for BBO, with  $L_z = 5\text{mm}$  and  $L_z = 2\text{mm}$ , both crystals pumped with  $\lambda_p = 351\text{nm}$ .

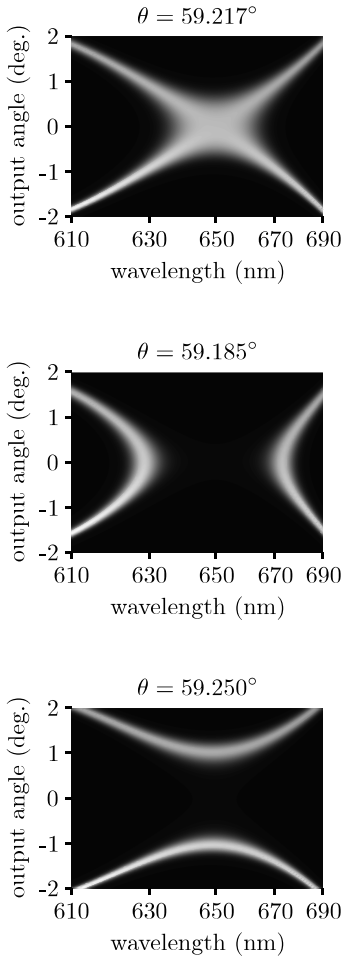


FIG. 6: Output angle in the  $xz$  plane as a function of the down-converted wavelength for a 15mm-long Lithium Iodate crystal pumped by a 325nm laser beam, for different values of the phase matching angle  $\theta$ . These results were obtained from Eqs. (26) and (27) integrating in  $\xi_2$  with  $\xi_{1y} = 0$ . The (nonlinear) horizontal scale was adjusted to allow a direct comparison with experimental data reported by Bogdanov *et al.* [34].

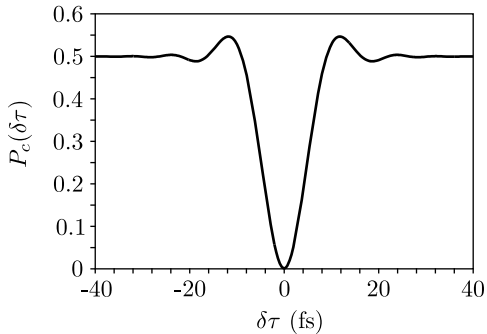


FIG. 7: Hong-Ou-Mandel dip for a 1mm-long BBO crystal cut for type I phase matching, with  $\theta = 34^\circ$  pumped by a 351nm laser, calculated with Eqs. (26) and (28). It is assumed that no interference filters are used.

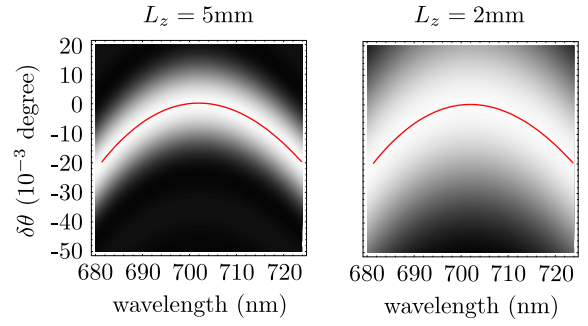


FIG. 8: (Color online) Down-converted wavelengths for collinear ( $\xi_1 = \xi_2 = 0$ ) type I phase matching as a function of  $\delta\theta$ , the deviation from  $\theta_m = 51.704^\circ$  for Lithium Iodate with  $L_z = 5\text{mm}$  (left) and  $L_z = 2\text{mm}$  (right), pumped with  $\lambda_p = 351\text{nm}$ . The solid line corresponds to the condition  $\mu_{oo}=0$ .

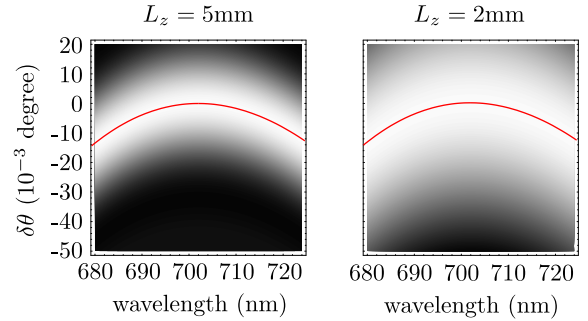


FIG. 9: (Color online) Down-converted wavelengths for collinear ( $\xi_1 = \xi_2 = 0$ ) type I phase matching as a function of  $\delta\theta$ , the deviation from  $\theta_m = 33.543^\circ$  for BBO with  $L_z = 5\text{mm}$  (left) and  $L_z = 2\text{mm}$  (right), pumped with  $\lambda_p = 351\text{nm}$ . The solid line corresponds to the condition  $\mu_{oo}=0$ .

Another useful representation of  $\Phi_{oo}$  is obtained when the following new coordinates are used:

$$\xi_s = \frac{1}{2}(\xi_1 + \xi_2), \quad (30a)$$

$$\xi_d = \frac{1}{2}(\xi_1 - \xi_2). \quad (30b)$$

Now, Eq.(26) is written as

$$\begin{aligned} \Phi_{oo} &\approx NG(\nu) \tilde{\mathcal{E}}(K\xi_s + K\nu\xi_d) \\ &\times \text{sinc} \left[ \frac{KL_z}{2} F_{oo}(\xi_s, \xi_d, \nu) \right] \\ &\times \exp[-iKz_c F_{oo}(\xi_s, \xi_d, \nu)], \end{aligned} \quad (31)$$

where  $N$  is a normalization constant and

$$\begin{aligned} F_{oo}(\xi_s, \xi_d, \nu) &= \mu_{oo} + \alpha_p(\xi_{sx} + \nu\xi_{dx}) \\ &- \frac{1}{2\bar{n}_o} [(1-b)\xi_{sx}^2 + (1-g)\xi_{sy}^2 + \xi_d^2 \\ &+ (2-b)\nu\xi_{sx}\xi_{dx} + (2-g)\nu\xi_{sy}\xi_{dy}], \end{aligned} \quad (32)$$

where  $\nu^2$  was neglected with respect to  $\nu$ .

Many of the interesting features of  $\Phi_{oo}$  are retained when the anisotropy is neglected in second order, that is, when the parameters  $a$  and  $b$  are both approximated by 1. In this case,

$$F_{oo}(\xi_s, \xi_d, \nu) \approx \mu_{oo} + \alpha_p(\xi_{sx} + \nu\xi_{dx}) - \frac{1}{2\bar{n}_o}(\xi_d^2 + \nu\xi_s \cdot \xi_d). \quad (33)$$

In the frequency degenerate case ( $\nu = 0$ ),

$$F_{oo}(\xi_s, \xi_d, \nu) \approx \mu_{oo} + \alpha_p\xi_{sx} - \frac{\xi_d^2}{2\bar{n}_o}. \quad (34)$$

Let us analyze the behavior of Eqs. (31) and (34) in two different measurement schemes: (a) When the detectors are scanned in opposite directions in the far field, so that  $\xi_s = 0$ . The probability of coincidence detection is proportional to

$$|\Phi_{oo}|_d^2 \approx \left| N G(\nu) \tilde{\mathcal{E}}(0) \text{sinc} \left[ \frac{KL_z}{4\bar{n}_o} (R^2 - \xi_d^2) \right] \right|^2. \quad (35)$$

Eq. (35) describes a circular profile in the variable  $\xi_d$ , with a radius  $R = \sqrt{2\bar{n}_o\mu_{oo}}$  and a half-width  $\delta R = \sqrt{R^2 + 4\pi\bar{n}_o/KL_z} - R$ . Under these detection conditions, the coincidence transverse profile maps the well-known down-converted light cones.

(b) When the detectors are scanned in the same direction in the far field, so that  $|\xi_d| = R$ . This condition means

$$|\Phi_{oo}|_s^2 \approx \left| N G(\nu) \tilde{\mathcal{E}}(K\xi_s) \text{sinc} \left( \frac{1}{2}KL_z\alpha_p\xi_{sx} \right) \right|^2. \quad (36)$$

Eq. (36) illustrates the possibility of transferring the angular spectrum  $\tilde{\mathcal{E}}(\mathbf{q})$  from the pump beam to the down-converted field  $\tilde{\mathcal{E}}(K\xi_s) = \tilde{\mathcal{E}}(\mathbf{q}_1 + \mathbf{q}_2)$  [30], and its dependence on the crystal length  $L_z$ . The sinc function has a half-width  $\delta\xi_{sx} = 2\pi/KL_z\alpha_p$  in the  $x$  direction. Depending on the spatial bandwidth of the pump beam, this factor may limit the transfer of its angular spectrum to the two-photon field. Considering that the pump beam is Gaussian, the transfer will be satisfactory only when its waist  $w_0$  is much larger than  $L_z\alpha_p/2\pi$ . For a BBO of  $L_z \sim 1\text{mm}$ ,  $L_z\alpha_p/2\pi \sim 10\mu\text{m}$ . This ‘‘clipping’’ in the angular spectrum transfer, caused by the walk-off term  $\alpha_p\xi_{sx}$ , has consequences in the anisotropy of entanglement in spatial variables of the two-photon state [36]. Figs. 10 and 11 show a comparison between experimental results obtained in our labs and the predictions of Eq. (36) for a BBO crystal with  $L_z = 5\text{mm}$  in collinear type I phase matching, pumped by a 405nm laser with  $w_0 \approx 25\mu\text{m}$ . In Fig. 10, the two detectors are scanned in the same sense, along the  $x$  direction. The effect of the walk-off term is evident. The dashed line shows the expected angular profile of the pump beam. In Fig. 11, the two detectors are scanned in the same sense, along the  $y$  direction. In both cases, interference filters of FWHM=10nm were used in front of the detectors.

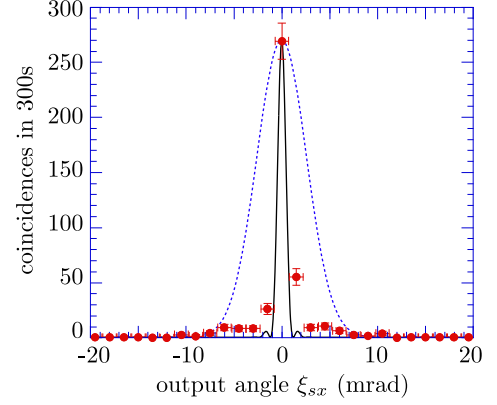


FIG. 10: (Color online) Comparison between experimental results ( $\bullet$ ) and the prediction of Eq. (36) (solid line) for a BBO crystal with  $L_z = 5\text{mm}$  in collinear type I phase matching, pumped by a 405nm laser with  $w_0 \approx 25\mu\text{m}$ . The two detectors are scanned in the same sense, along the  $x$  direction. The dashed line shows a gaussian profile corresponding to the pump laser beam.

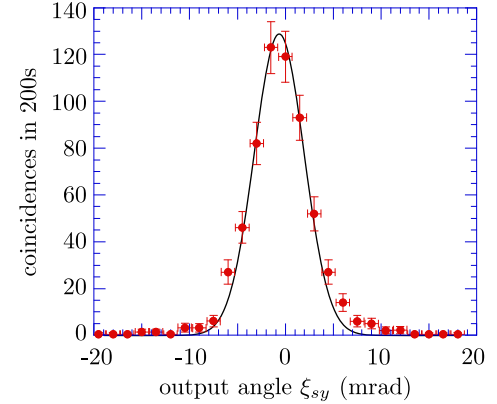


FIG. 11: (Color online) Comparison between experimental results ( $\bullet$ ) and the prediction of Eq. (36) (solid line) for a BBO crystal with  $L_z = 5\text{mm}$  in collinear type I phase matching, pumped by a 405nm laser with  $w_0 \approx 25\mu\text{m}$ . The two detectors are scanned in the same sense, along the  $y$  direction. The Gaussian predicted by Eq.(36) coincides with the expected profile of the pump beam.

## V. TYPE II PHASE MATCHING

In type II phase matching, the calculation is similar, except for the fact that one of the down-converted beams has extraordinary polarization ( $e \rightarrow oe$  or  $e \rightarrow eo$ ), that is,

$$|\Psi\rangle = \int d\nu \int d\mathbf{q}_1 \int d\mathbf{q}_2 [\Phi_{oe} |\mathbf{q}_1, \nu; o\rangle |\mathbf{q}_2, -\nu; e\rangle + \Phi_{eo} |\mathbf{q}_1, \nu; e\rangle |\mathbf{q}_2, -\nu; o\rangle]. \quad (37)$$

Now, the  $k_z$  component of the  $e$ -polarized down-converted wave has to be written according to expression (16), that is, for the case  $e \rightarrow oe$ ,

$$k_{pz} \approx \varkappa_p - \alpha_p q_{px} - \frac{1}{2\varkappa_p}(\beta_p q_{px}^2 + \gamma_p q_{py}^2), \quad (38)$$

$$k_{1z} \approx k_1 - \frac{q_1^2}{2k_1}, \quad (39)$$

$$k_{2z} \approx \varkappa_2 - \bar{\alpha} q_{2x} - \frac{1}{2\varkappa_2}(\bar{\beta} q_{2x}^2 + \bar{\gamma} q_{2y}^2), \quad (40)$$

where  $k_1 = \bar{n}_o(1 + a\nu)(1 + \nu)\omega_p/2c$  and  $\varkappa_2 = \bar{\eta}(1 - a'\nu)(1 - \nu)\omega_p/2c$ . The factor  $a'$  is defined analogous to Eq. (21), replacing  $n_o$  by  $\eta$ .  $\bar{\alpha}$ ,  $\bar{\beta}$ ,  $\bar{\gamma}$  and  $\bar{\eta}$  are calculated with  $n_o$  and  $n_e$  taken at  $\omega_p/2$ .

The amplitudes  $\Phi_{oe}$  and  $\Phi_{eo}$  have expressions analogous to Eq. (5), with  $\Delta_z^{oe}$  and  $\Delta_z^{eo}$  given by

$$\begin{aligned} \Delta_z^{oe} = & K\mu_{oe} + \alpha_p q_{1x} + (\alpha_p - \bar{\alpha})q_{2x} \\ & + \frac{1}{\bar{n}_o K} \left[ \frac{b}{2}(q_{1x} + q_{2x})^2 + \frac{g}{2}(q_{1y} + q_{2y})^2 \right. \\ & \left. - \bar{b}q_{2x}^2 - \bar{g}q_{2y}^2 - q_1^2 + (q_1^2 - \bar{b}q_{2x}^2 - \bar{g}q_{2y}^2)\nu \right], \quad (41a) \end{aligned}$$

$$\begin{aligned} \Delta_z^{eo} = & K\mu_{eo} + (\alpha_p - \bar{\alpha})q_{1x} + \alpha_p q_{2x} \\ & + \frac{1}{\bar{n}_o K} \left[ \frac{b}{2}(q_{1x} + q_{2x})^2 + \frac{g}{2}(q_{1y} + q_{2y})^2 \right. \\ & \left. - \bar{b}q_{1x}^2 - \bar{g}q_{1y}^2 - q_2^2 + (q_2^2 - \bar{b}q_{1x}^2 - \bar{g}q_{1y}^2)\nu \right], \quad (41b) \end{aligned}$$

where

$$\mu_{oe} = \frac{\bar{n}_o + \bar{\eta}}{2} - \eta_p + \nu \frac{\bar{n}_o - \bar{\eta}}{2}, \quad (42a)$$

$$\mu_{eo} = \frac{\bar{n}_o + \bar{\eta}}{2} - \eta_p - \nu \frac{\bar{n}_o - \bar{\eta}}{2}, \quad (42b)$$

$b = \beta_p \bar{n}_o / \eta_p$ ,  $g = \gamma_p \bar{n}_o / \eta_p$ ,  $\bar{b} = \bar{\beta} \bar{n}_o / \bar{\eta}$ ,  $\bar{g} = \bar{\gamma} \bar{n}_o / \bar{\eta}$ , and  $q_1^2 = |\mathbf{q}_1|^2$ . In Eqs. (41), terms in  $a$  and  $a'$  were neglected with respect to 1, and  $\nu^2$  was neglected with respect to  $\nu$ . Note that  $\mu_{oe}$  and  $\mu_{eo}$  have a linear dependence on  $\nu$ , differently from  $\mu_{oo}$ , whose dependence is on  $\nu^2$ .

In terms of the output angles  $\xi_1$  and  $\xi_2$ , we have

$$\begin{aligned} \Phi_{oe} \approx & N G(\nu) \tilde{\mathcal{E}} \left[ \frac{K}{2}(\xi_1 + \xi_2) + \frac{K\nu}{2}(\xi_1 - \xi_2) \right] \\ & \times \text{sinc} \left[ \frac{KL_z}{2} f_{oe}(\xi_1, \xi_2, \nu) \right] \\ & \times \exp[-iKz_c f_{oe}(\xi_1, \xi_2, \nu)], \quad (43) \end{aligned}$$

where  $N$  is a normalization constant and

$$\begin{aligned} f_{oe} = & \mu_{oe} + \frac{\alpha_p}{2}(1 + \nu)\xi_{1x} + \frac{\alpha_p - \bar{\alpha}}{2}(1 - \nu)\xi_{2x} \\ & - \frac{1}{4\bar{n}_o} \left\{ (1 + \nu)\xi_1^2 + (1 - \nu)(\bar{b}\xi_{2x}^2 + \bar{g}\xi_{2y}^2) \right. \\ & - \frac{b}{2}[(1 + \nu)\xi_{1x} + (1 - \nu)\xi_{2x}]^2 \\ & \left. - \frac{g}{2}[(1 + \nu)\xi_{1y} + (1 - \nu)\xi_{2y}]^2 \right\}. \quad (44) \end{aligned}$$

$\Phi_{eo}$  has an expression similar to (43), with

$$\begin{aligned} f_{eo} = & \mu_{eo} + \frac{\alpha_p - \bar{\alpha}}{2}(1 + \nu)\xi_{1x} + \frac{\alpha_p}{2}(1 - \nu)\xi_{2x} \\ & - \frac{1}{4\bar{n}_o} \left\{ (1 + \nu)(\bar{b}\xi_{1x}^2 + \bar{g}\xi_{1y}^2) + (1 - \nu)\xi_2^2 \right. \\ & - \frac{b}{2}[(1 + \nu)\xi_{1x} + (1 - \nu)\xi_{2x}]^2 \\ & \left. - \frac{g}{2}[(1 + \nu)\xi_{1y} + (1 - \nu)\xi_{2y}]^2 \right\}. \quad (45) \end{aligned}$$

Fig. 12 shows density plots of single counts obtained from Eqs. (43-45) integrated in one of the output angles and in  $\nu$  over a bandwidth of 0.025 (corresponding to a 10nm filter) for a BBO crystal pumped by a 407nm laser, cut for  $\theta = 42.5^\circ$ , with  $L_z = 1\text{mm}$  (left) and  $L_z = 0.25\text{mm}$  (right). Both plots are in good agreement with experimental data reported by Lee *et al.* [11].

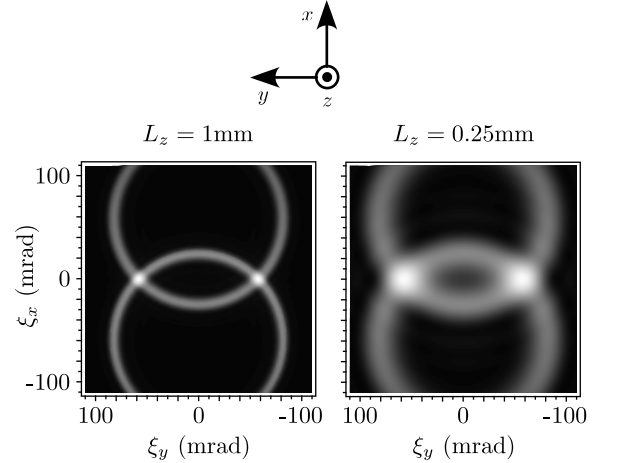


FIG. 12: Density plot of single counts obtained from Eq. (47) integrated in one of the output angles and in  $\nu$  over a bandwidth of 0.025 (which corresponds to a 10nm filter) for a BBO crystal pumped by a 407nm laser, cut for  $\theta = 42.5^\circ$ , with  $L_z = 1\text{mm}$  (left) and  $L_z = 0.25\text{mm}$  (right).

The linear dependence of  $\mu_{oe}$  and  $\mu_{eo}$  with  $\nu$  leads to a frequency spectrum of the two-photon state quite different from the type I case. Figure 13 shows the down-converted wavelengths for collinear ( $\xi_1 = \xi_2 = 0$ ) type II phase matching as a function of  $\delta\theta$ , the deviation from  $\theta_m = 49.223^\circ$  for BBO with  $L_z = 5\text{mm}$  and  $L_z = 2\text{mm}$ , pumped with  $\lambda_p = 351\text{nm}$ . Both plots were obtained from Eqs (43-45).

Fig. 14 shows the Hong-Ou-Mandel dip for a 1mm-long BBO crystal cut for *beamlike* type II phase matching ( $\theta = 48.34^\circ$ ), pumped by a 351nm laser. The solid line corresponds to the case in which interference filters of 20nm bandwidth are used, in good agreement with the data reported by Kim [37]. The dashed line corresponds to the case in which no interference filters are used. Notice the difference between Figs. 7 and 14. In type II phase matching, the Hong-Ou-Mandel dip is much larger



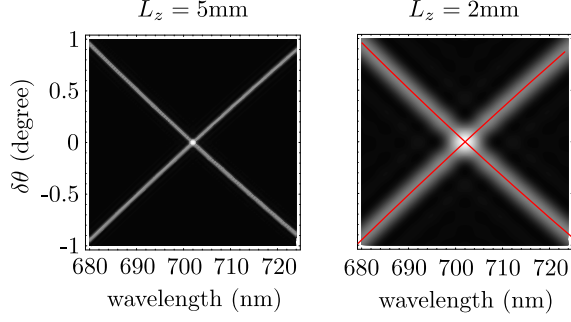


FIG. 13: (Color online) Down-converted wavelengths for collinear ( $\xi_1 = \xi_2 = 0$ ) type II phase matching as a function of  $\delta\theta$ , the deviation from  $\theta_m = 49.223^\circ$  for BBO with  $L_z = 5\text{mm}$  (left) and  $L_z = 2\text{mm}$  (right), pumped with  $\lambda_p = 351\text{nm}$ . The solid lines correspond to the conditions  $\mu_{oe}=0$  and  $\mu_{eo}=0$ .

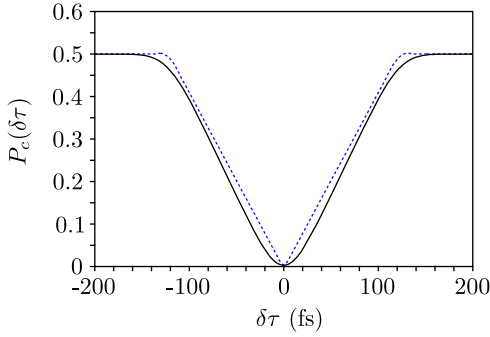


FIG. 14: (Color online) Hong-Ou-Mandel dip for a 1mm-long BBO crystal cut for type II phase matching, with  $\theta = 48.34^\circ$  pumped by a 351nm laser, calculated with Eqs. (28) and (43). The solid line corresponds to the case in which interference filters of 20nm bandwidth are used. The dashed line corresponds to the case in which no interference filters are used.

than in type I, indicating a narrower frequency spectrum in type II.

It is also possible to write  $\Phi_{oe}$  and  $\Phi_{eo}$  in terms of the variables  $\xi_s$  and  $\xi_d$  defined in Eq. 30, but the exact expressions are too long to be of practical use. However, when  $b, \bar{b}, g$  and  $\bar{g}$  are all approximated by 1, we arrive at the useful expressions

$$F_{oe} = \mu_{oe} + \left(\alpha_p - \frac{1+\nu}{2}\bar{\alpha}\right)\xi_{sx} + \left(\nu\alpha_p + \frac{1-\nu}{2}\bar{\alpha}\right)\xi_{dx} - \frac{\xi_d^2}{2\bar{n}_o}, \quad (46a)$$

$$F_{eo} = \mu_{eo} + \left(\alpha_p - \frac{1-\nu}{2}\bar{\alpha}\right)\xi_{sx} + \left(\nu\alpha_p - \frac{1+\nu}{2}\bar{\alpha}\right)\xi_{dx} - \frac{\xi_d^2}{2\bar{n}_o}. \quad (46b)$$

When the detectors are scanned in opposite directions in the far field, so that  $\xi_s = 0$ , the probability of coincidence

detection  $P_d$  is proportional to  $\int d\nu (|\Phi_{oe}|_d^2 + |\Phi_{eo}|_d^2)$ , where

$$|\Phi_{oe}|_d^2 \approx |NG(\nu)\tilde{\mathcal{E}}(0)|^2 \times \text{sinc}^2\left[\frac{KL}{4\bar{n}_o}(R_{oe}^2 - |\xi_d - \mathbf{c}_{oe}|^2)\right], \quad (47a)$$

$$|\Phi_{eo}|_d^2 \approx |NG(\nu)\tilde{\mathcal{E}}(0)|^2 \times \text{sinc}^2\left[\frac{KL}{4\bar{n}_o}(R_{eo}^2 - |\xi_d - \mathbf{c}_{eo}|^2)\right], \quad (47b)$$

$$R_{oe}^2 = 2\bar{n}_o\mu_{oe} + \bar{n}_o^2\bar{\alpha}^2\left[\frac{1}{4} - \nu\left(\frac{\alpha_p}{\bar{\alpha}} - \frac{1}{2}\right)\right], \quad (48a)$$

$$R_{eo}^2 = 2\bar{n}_o\mu_{eo} + \bar{n}_o^2\bar{\alpha}^2\left[\frac{1}{4} + \nu\left(\frac{\alpha_p}{\bar{\alpha}} - \frac{1}{2}\right)\right], \quad (48b)$$

$$\mathbf{c}_{oe} = \bar{n}_o\bar{\alpha}\left[\frac{1}{2} + \nu\left(\frac{\alpha_p}{\bar{\alpha}} - \frac{1}{2}\right)\right]\hat{\mathbf{x}}, \quad (49a)$$

$$\mathbf{c}_{eo} = \bar{n}_o\bar{\alpha}\left[-\frac{1}{2} + \nu\left(\frac{\alpha_p}{\bar{\alpha}} - \frac{1}{2}\right)\right]\hat{\mathbf{x}}, \quad (49b)$$

and  $\hat{\mathbf{x}}$  is the unit vector in the  $x$  direction.

Expressions (47) describe two circular profiles, centered at  $\xi_d = \mathbf{c}_{oe}$  and  $\xi_d = \mathbf{c}_{eo}$ , with radii  $R_{oe}$  and  $R_{eo}$ , respectively. Collinear down-conversion occurs when  $R_{oe} = c_{oe}$  and  $R_{eo} = c_{eo}$ . The so-called *beamlike* type II down-conversion occurs in the degenerate case ( $\nu = 0$ ) when  $\theta$  is such that  $R_{oe} = R_{eo} = 0$ .

Let us analyze the case when the detectors are scanned in the same direction in the far field, so that  $\xi_d = 0$ . Then,

$$|\Phi_{oe}|_s^2 \approx |NG(\nu)\tilde{\mathcal{E}}(K\xi_s)|^2 \times \text{sinc}^2\left\{\frac{KL_z}{2}\left[\mu_{oe} + \left(\alpha_p - \frac{\bar{\alpha}}{2}\right)\xi_{sx}\right]\right\}, \quad (50a)$$

$$|\Phi_{eo}|_s^2 \approx |NG(\nu)\tilde{\mathcal{E}}(K\xi_s)|^2 \times \text{sinc}^2\left\{\frac{KL_z}{2}\left[\mu_{eo} + \left(\alpha_p - \frac{\bar{\alpha}}{2}\right)\xi_{sx}\right]\right\}. \quad (50b)$$

Note that in type II the transfer of angular spectrum described by Eqs. (50) is affected by the detuning  $\nu$  through the parameters  $\mu_{oe}$  and  $\mu_{eo}$ . The detuning has the effect of displacing the sinc function by an amount  $(\bar{n}_o - \bar{\eta})KL_z\nu/4$  in the  $x$  axis, in opposite directions for  $|\Phi_{oe}|_s^2$  and  $|\Phi_{eo}|_s^2$ . In the limit of long crystals, the sinc<sup>2</sup> functions are narrow enough to allow us to write the coincidence detection probability as

$$P_s = \int d\nu (|\Phi_{oe}|_s^2 + |\Phi_{eo}|_s^2) \approx |N\tilde{\mathcal{E}}(K\xi_s)|^2 \left[G^2\left(-\frac{\xi_{sx}}{m}\right) + G^2\left(\frac{\xi_{sx}}{m}\right)\right], \quad (51)$$

where  $m = (2\alpha_p - \bar{\alpha})/(\bar{n}_o - \bar{\eta})$ . In type II phase matching, due to the linear dependence of  $\mu_{oe}$  and  $\mu_{eo}$  on  $\nu$ ,

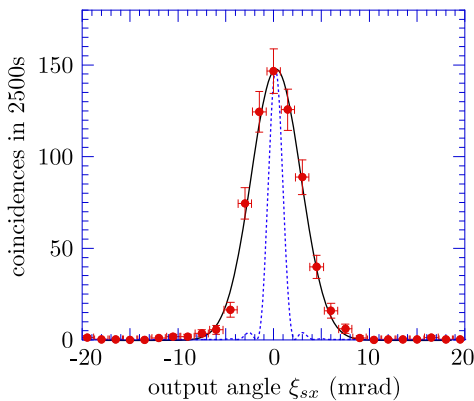


FIG. 15: (Color online) Comparison between experimental results ( $\bullet$ ) and the prediction of Eq. (50) (solid line) for a BBO crystal with  $L_z = 5\text{mm}$  in collinear type II phase matching, pumped by a 405nm laser with  $w_0 \approx 25\mu\text{m}$ . The two detectors are scanned in the same sense, along the  $x$  direction. The Gaussian predicted by Eq.(50) coincides with the expected profile of the pump beam. The dashed line shows the expected curve for the monochromatic case.

the angular spectrum of the pump field may be transferred to the two-photon state if the bandwidth of the detection filters is broad enough, even for long crystals. Figs. 15 and 16 show comparison of the predictions of Eq. (50) with experimental data for a 5mm-long BBO crystal pumped by a 405nm laser with  $w_0 \approx 25\mu\text{m}$  and detection filters with a bandwidth of 10nm. In both figures, there is a good agreement between experimental data and the expected Gaussian profile of the pump beam. The experimental conditions are the same of Figs. 10 and 11, except for the phase matching type. Notice the difference between the two cases when the detectors are scanned in the  $x$  direction (Figs. 10 and 15). In the case of Fig. 15, the 10nm filter allows a complete transfer of the pump beam profile to the coincidence detection. The dashed line shows the expected curve for the monochromatic case, that is,  $G(\nu) \approx \delta(\nu)$  (zero bandwidth filter).

## VI. SUMMARY AND CONCLUSION

We have discussed in detail the two-photon state generated by spontaneous parametric down-conversion in bulk crystals, taking into account the effect of crystal anisotropy, in both in type I and type II phase matching. Our discussion was based on the perturbative ap-

proach introduced by Hong and Mandel, in the context of Fourier Optics, in which the fields are treated by means of their plane-wave expansion. The frequency spectrum of the down-converted fields was also considered, in the approximation of small detuning and monochromatic pump beams. Extension of the theory to cover pulsed pump

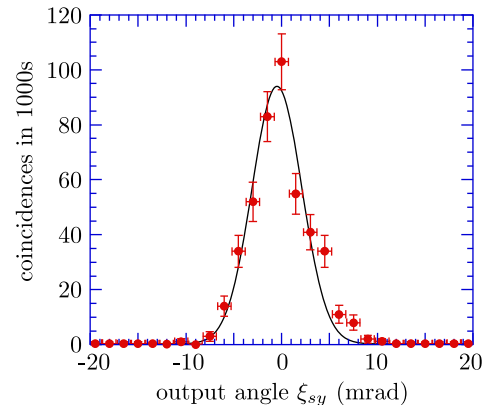


FIG. 16: (Color online) Comparison between experimental results ( $\bullet$ ) and the prediction of Eq. (50) (solid line) for a BBO crystal with  $L_z = 5\text{mm}$  in collinear type II phase matching, pumped by a 405nm laser with  $w_0 \approx 25\mu\text{m}$ . The two detectors are scanned in the same sense, along the  $y$  direction. The Gaussian predicted by Eq.(50) coincides with the expected profile of the pump beam.

beams seems straightforward. Several approximations were made in order to provide simple expressions that still exhibit the main features of the frequency and spatial spectral properties of the two-photon states. These expressions were shown to be in good agreement with experimental data for some selected situations. In particular, the spectral content of the two-photon state and the transfer of angular spectrum from the pump beam to the two-photon state were analyzed, and a significant differences of these features in type I and type II phase matching were discussed. The results presented here are a contribution to the Fourier optics of two-photon states and may be helpful to improve the understanding and further development of entangled state sources for quantum information and quantum communication.

## Acknowledgments

This work was supported by the Brazilian funding agencies CNPq, CAPES and FAPEMIG.

[1] L. Mandel, Ann. N. Y. Acad. Sci. **755**, 1 (1995).  
 [2] Y. H. Shih, A. V. Sergienko, T. B. Pittman, and M. Ru-

bin, Ann. N. Y. Acad. Sci. **755**, 40 (1995).  
 [3] A. Zeilinger, Rev. Mod. Phys. **71**, 288 (1999).

- [4] A. G. White, D. F. V. James, W. J. Munro, and P. G. Kwiat, *Phys. Rev. A* **65**, 012301 (2001).
- [5] P. G. Kwiat, K. Mattle, H. Weinfurter, A. Zeilinger, A. V. Sergienko, and Y. Shih, *Phys. Rev. Lett.* **75**, 4337 (1995).
- [6] P. G. Kwiat, E. Waks, A. G. White, I. Appelbaum, and P. H. Eberhard, *Phys. Rev. A* **60**, 773 (1999).
- [7] C. Kurtsiefer, M. Oberparleiter, and H. Weinfurter, *Phys. Rev. A* **64**, 023802 (2001).
- [8] G. Bitton, W. P. Grice, J. Moreau, and L. Zhang, *Phys. Rev. A* **65**, 063805 (2002).
- [9] J. B. Altepeter, E. R. Jeffrey, and P. G. Kwiat, *Opt. Expr.* **13**, 8951 (2005).
- [10] M. Barbieri, C. Cinelli, F. D. Martini, and P. Mataloni, *Eur. Phys. J. D* **32**, 261 (2005).
- [11] P. S. K. Lee, M. P. van Exter, and J. P. Woerdman, *Phys. Rev. A* **70**, 043818 (2004).
- [12] Y. Shih, *Rep. Prog. Phys.* **66**, 1009 (2003).
- [13] H. H. Arnaut and G. A. Barbosa, *Phys. Rev. Lett.* **85**, 286 (2000).
- [14] S. Franke-Arnold, S. M. Barnett, M. J. Padgett, and L. Allen, *Phys. Rev. A* **65**, 033823 (2002).
- [15] G. A. Barbosa and H. H. Arnaut, *Phys. Rev. A* **65**, 053801 (2002).
- [16] S. P. Walborn, A. N. de Oliveira, R. S. Thebaldi, and C. H. Monken, *Phys. Rev. A* **69**, 023811 (2004).
- [17] J. P. Torres, C. Molina-Terriza, and L. Torner, *J. Opt. B* **7**, 235 (2005).
- [18] G. A. Barbosa, *Phys. Rev. A* **76**, 033821 (2007).
- [19] C. Osorio, C. Molina-Terriza, and J. P. Torres, *Phys. Rev. A* **77**, 15810 (2008).
- [20] C. K. Hong and L. Mandel, *Phys. Rev. A* **31**, 2409 (1985).
- [21] D. N. Klyshko, *Sov. Phys. JETP* **28**, 522 (1969).
- [22] M. Rubin, *Phys. Rev. A* **54**, 5349 (1996).
- [23] J. P. Torres, C. I. Osorio, and L. Torner, *Opt. Lett.* **29**, 1939 (2004).
- [24] M. V. Fedorov, M. A. Efremov, P. A. Volkov, E. V. Moreva, S. S. Straupe, and S. P. Kulik, *Phys. Rev. A* **77**, 032336 (2008).
- [25] S.-Y. Baek and Y.-H. Kim, *Phys. Rev. A* **77**, 043807 (2008).
- [26] T. G. Giallorenzi and C. L. Tang, *Phys. Rev.* **166**, 225 (1968).
- [27] A. Joobeur, B. Saleh, and M. Teich, *Phys. Rev. A* **50**, 3349 (1994).
- [28] C. Kurtsiefer, M. Oberparleiter, and H. Weinfurter, *J. Mod. Opt.* **48**, 1997 (2001).
- [29] L. Mandel and E. Wolf, *Optical Coherence and Quantum Optics* (Cambridge University Press, 1995).
- [30] C. H. Monken, P. H. S. Ribeiro, and S. Pádua, *Phys. Rev. A* **57**, 3123 (1998).
- [31] M. Born and E. Wolf, *Principles of Optics* (Cambridge University Press, 1999).
- [32] V. G. Dmitiev, G. G. Gurzadyan, and D. N. Nikogosyan, *Handbook of Nonlinear Optical Crystals* (Springer-Verlag, 1997).
- [33] Sellmeier equations for Lithium Iodate change from manufacturer to manufacturer.
- [34] Y. I. Bogdanov, E. V. Moreva, G. A. Maslennikov, R. F. Galeev, S. S. Straupe, and S. P. Kulik, *Phys. Rev. A* **73**, 063810 (2006).
- [35] C. K. Hong, Z. Y. Ou, and L. Mandel, *Phys. Rev. Lett.* **59**, 2044 (1987).
- [36] M. V. Fedorov, M. A. Efremov, P. A. Volkov, E. V. Moreva, S. S. Straupe, and S. P. Kulik, *Phys. Rev. Lett.* **99**, 063901 (2007).
- [37] Y.-H. Kim, *Phys. Rev. A* **68**, 013804 (2003).